



## Fabrication of cell penetration enhanced poly (L-lactic acid-co-ε-caprolactone)/silk vascular scaffolds utilizing air-impedance electrospinning

Anlin Yin<sup>a</sup>, Jiukai Li<sup>b</sup>, Gary L. Bowlin<sup>c</sup>, Dawei Li<sup>a</sup>, Isaac A. Rodriguez<sup>c</sup>, Jing Wang<sup>a</sup>, Tong Wu<sup>a</sup>, Hany A. El-Hamshary<sup>d,e</sup>, Salem S. Al-Deyab<sup>d</sup>, Xiumei Mo<sup>a,d,\*</sup>

<sup>a</sup> College of Chemistry, Chemical Engineering and Biotechnology, Donghua University, Shanghai 201620, China

<sup>b</sup> College of Architecture and Environment, Sichuan University, Chengdu 610065, China

<sup>c</sup> Department of Biomedical Engineering, University of Memphis, Memphis, Tennessee, TN 38152, USA

<sup>d</sup> Department of Chemistry, College of Science, King Saud University, Riyadh 11451, Saudi Arabia

<sup>e</sup> Department of Chemistry, Faculty of Science, Tanta University, Tanta 31527, Egypt

### ARTICLE INFO

#### Article history:

Received 17 December 2013

Received in revised form 13 March 2014

Accepted 17 April 2014

Available online 22 May 2014

#### Keywords:

Vascular tissue engineering

Vascular prosthetic

Cell infiltration

Electrospinning

### ABSTRACT

In the vascular prosthetic field, the prevailing thought is that for clinical, long-term success, especially bioresorbable grafts, cellular migration and penetration into the prosthetic structure is required to promote neointima formation and vascular wall development. In this study, we fabricated poly (L-lactic acid-co-ε-caprolactone) P(LLA-CL)/silk fibroin (SF) vascular scaffolds through electrospinning using both perforated mandrel subjected to various intraluminal air pressures (0–300 kPa), and solid mandrel. The scaffolds were evaluated the cellular infiltration *in vitro* and mechanical properties. Vascular scaffolds were seeded with smooth muscle cells (SMCs) to evaluate cellular infiltration at 1, 7, and 14 days. The results revealed that air-impedance scaffolds allowed significantly more cell infiltration as compared to the scaffolds fabricated with solid mandrel. Meanwhile, results showed that both mandrel model and applied air pressure determined the interfiber distance and the alignment of fibers in the enhanced porosity regions of the structure which influenced cell infiltration. Uniaxial tensile testing indicated that the air-impedance scaffolds have sufficient ultimate strength, suture retention strength, and burst pressure as well as compliance approximating a native artery. In conclusion, the air-impedance scaffolds improved cellular infiltration without compromising overall biomechanical properties. These results support the scaffold's potential for vascular grafting and *in situ* regeneration.

© 2014 Elsevier B.V. All rights reserved.

### 1. Introduction

In 2009, there were 416,000 surgical procedures performed involving coronary artery bypass surgery in USA as an example of the clinical need for small diameter (<6 mm inner diameter (I.D.)) vascular grafts [1]. Today, the saphenous vein remains the gold standard to replace diseased vascular tissue, but it may not be suitable for some patients because of vascular disease, amputation and previous harvest. Additionally, the use of this vein requires a secondary surgical procedure to obtain the vessel [2–5].

Due to limited autologous vessels for grafting, synthetic vascular prosthetics composed of Dacron (polyethylene terephthalate (PET)) and expanded polytetrafluorethylene (ePTFE) were developed but have had limited success when used as small-diameter arterial substitutes whereas these materials as large-caliber arterial substitutes have succeeded. The reason for this limited success is lower blood flow velocities and increased flow resistance within these smaller vascular grafts leading to the failure modes of acute thrombogenicity and anastomotic/intimal hyperplasia. Thus, there remains a clear clinical need for a functional small-diameter arterial graft. Tissue engineered blood vessels (TEBV) are promising alternatives as a method of treatment for blood vessel defects. Over the past two decades, much effort has therefore been devoted to developing a viable TEBV in terms of biomechanical and biological performance, however with limited success [6].

\* Corresponding author at: Biomaterials and Tissue Engineering Lab, College of Chemistry, Chemical Engineering and Biotechnology, Donghua University, Rm 4091 No.4 College Building, Shanghai 201620, PR China. Tel.: +86 021 67786523.

E-mail address: [xmm@dhu.edu.cn](mailto:xmm@dhu.edu.cn) (X. Mo).

Electrospinning is an attractive process which can generate micro- to nano-fibrous vascular scaffolds with a high surface area to volume ratio mimicking the architecture of the natural extracellular matrix (ECM) [7]. Moreover, electrospinning affords the opportunity to incorporate drugs, growth factors and other biomolecular signals into the polymeric solutions before electrospinning. A variety of natural and synthetic biodegradable polymers have been electrospun as manufacturing materials for the fabrication of scaffolds, such as collagen [8], elastin [9], silk fibroin [10–12], chitosan [8,10,13] and synthetics including poly(lactic acid) (PLA) [14,15], poly(glycolic acid) (PGA) [16,17], polycaprolactone (PCL) [18], polydioxanone [19,20] and poly(L-lactic acid-co- $\epsilon$ -caprolactone) (P(LLA-CL)) [8,21]. Pore size, pore interconnectivity, and porosity are important characteristics for any scaffold to provide sufficient cell infiltration, exchange of nutrients and metabolic products of host cells, and three-dimensional (3-D) tissue regeneration [22,23]. However, a historic limitation of electrospinning is the inability to control the pore size and porosity of the scaffolds attributed to the random deposition of fibers. It is logical that cells should be distributed throughout the entire scaffold to allow for the development of a functional tissue engineered product. Thus, when fabricating a scaffolding to promote tissue regeneration, cell and capillary infiltration must occur with the pore size and interconnectivity determining success or failure [24].

In order to overcome the limitations of uncontrolled porosity and pore size that hinder cells from penetrating into electrospun scaffolds, several methods have been attempted to enhance cell infiltration upon seeding. Ju et al. developed a bilayered vascular scaffold where the inner layer yielded small diameter fibers and the outer layer consisted of large diameter fibers to provide different pore sizes to facilitate adequate cellular interactions [25]. The bilayered scaffolds permitted endothelial cells (EC) adhesion on the lumen and smooth muscle cells (SMC) infiltration into the outer layer. Wu et al. developed a novel nanoyarn scaffold by dynamic liquid electrospinning [26]. Through this method, aligned nanoyarns were fabricated and formed a 3-D scaffold. This scaffold possessed large pore sizes or interfiber distance and high porosity which facilitated cell infiltration into the structure. Baker et al. used water soluble polyethylene oxide (PEO) as sacrificial fibers intermingled with PCL fibers through electrospinning [27]. After immersing the PEO/PCL scaffolds into water, the PEO dissolved leaving only the PCL fibers, thus increasing the effective pore size of the scaffold, and enhancing cellular infiltration. Unfortunately, the mechanical properties of these scaffolds decreased significantly with increasing PEO composition.

In a previous study by Dr. Bowlin and associates, electrospun PCL grafts fabricated with porous mandrel were evaluated. During the air-impedance process, traditional solid mandrel was replaced with a perforated mandrel, and added pressurized air exiting the pores to impede fiber deposition. Through this procedure, air-impedance electrospun grafts possessed larger pore diameter (interfiber distance) and the fibers formed less compacted, this kind of graft structure allowed partially increased cellular infiltration in defined regions than on traditional electrospun fiber grafts [24].

In this study, an elastic material of P(LLA-CL) and natural protein of SF were used to fabricate P(LLA-CL)/SF vascular scaffolds, utilizing air-impedance electrospinning method. The air-impedance processing method uses air flow to impede fiber deposition onto the mandrel in a controlled, patterned fashion to increase the scaffold porosity. The fabricated scaffolds were characterized to determine their potential application as a vascular scaffold/prosthetic. This study explored cell penetration into the scaffold, and calculated the depth of cellular infiltration. Furthermore, scaffold mechanical properties were evaluated in terms of tensile testing, suture retention, burst pressure and compliance.

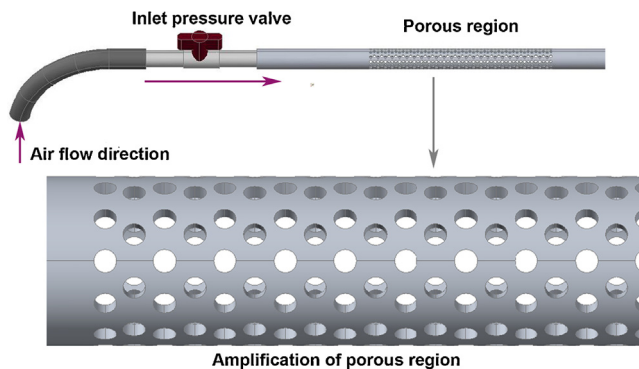


Fig. 1. Diagram of the prototype air-impedance mandrel.

## 2. Materials and methods

### 2.1. Silk fibroin extraction

SF was extracted from the cocoons of *Bombyx mori* silkworms (The Yarn Tree, NY, USA) by following a published protocol [28]. Briefly, cocoons were cut into pieces and boiled in a 0.02 M  $\text{Na}_2\text{CO}_3$  (Sigma Aldrich) solution for 30 min to remove the sericin gum, followed by thorough rinsing in de-ionized water (DI), the boiling and rinsing processes were repeated three times, and then air-dried overnight in a fume hood. The SF was then dissolved in a LiBr (Fisher Scientific) solution at 60 °C for 1 h, (1 g silk raw fiber dissolved in 4 mL (9.3 mole/L) LiBr solution). This solution was then dialyzed against deionized water for 3 days using 12,000–14,000 MWCO dialysis tubing (Fisher Scientific). The SF solution was then frozen and lyophilized to provide pure SF for electrospinning.

### 2.2. Electrospinning

A polymer of P (LLA-CL) (MW: 300,000, LA to CL mole ratio is 50:50, Gunze Limited, Japan) and SF were dissolved in 1,1,1,3,3,3-hexafluoro-2-propanol (HFP, TCI America) at 70 mg/mL, respectively. P(LLA-CL) and SF solution were blended at volume ratio of 70:30. To create vascular graft scaffolds, the blended solution was loaded into a 5 mL plastic Becton Dickinson syringe with a 16 ga blunt tip needle and dispensed at a rate of 5 mL/h. The needle tip was subjected to +30 kV with an air gap distance of 20 cm between the needle and the grounded mandrel. Electrospinning was performed on both solid and perforated stainless steel mandrels [24]. Fig. 1 is the sketch of perforated mandrel. The perforated mandrel was subjected to a luminal air pressure of 0, 50, 100, 200 and 300 kPa to determine the effect of a range of air-flow rates on fiber deposition and vascular graft structural properties.

### 2.3. Scaffold morphology characterization

Scaffold morphology characterization was performed using scanning electron microscopy (SEM, JEOL JSM-5610LV, Japan). SEM micrographs were analyzed with a software Image-J (National Institutes of Health). The average fiber diameter was determined by measuring 50 randomly selected fibers in the SEM image. Interfiber distance was measured by determining distance based on both the most superficial fibers and by measuring from one fiber to the next closest fiber (SEM image). Calibration of the Image Tool software was achieved by using the scale bar on each image. Moreover, we evaluated the alignment of fibers which typically deposited on solid and perforated mandrels (within pore regions) according to a previous procedure [29], a two-dimensional fast Fourier transform (2D FFT) approach. In brief, a quadrate region was captured from

SEM images and then analyzed with Image-J software to create corresponding frequency plots and 2D FFT alignment plots.

#### 2.4. Cellular analysis

In order to studying the infiltration and proliferation of cells on scaffolds, cells were seeded on the scaffolds. Air-impedance electrospun vascular scaffolds were seeded with human aortic smooth muscle cells (SMCs, Cascade Biologics). To culture SMCs, DMEM (Gibco) was supplemented with 10% fetal bovine serum (Hyclone), and 1% penicillin/streptomycin (Invitrogen). Scaffolds were placed into 48-well plates, disinfected by soaking in 90% ethanol (Sigma) for 30 min followed by three 10 min Phosphate Buffered Saline (PBS) washes, seeded with 100  $\mu$ L of the cell suspension (cell concentration of 200,000 cells/mL), and placed in an incubator at 37 °C and 5% CO<sub>2</sub> for 1, 7 and 14 days. Media was changed every 2 days.

After cellular interaction time periods, Cryosections were stained with 4',6-diamidino-2-phenylindole (DAPI, Invitrogen) for imaging and examination of cellular infiltration. Samples were first fixed using 10% buffered formalin for 24 h at 4 °C, then embedded in Optimal Cutting Temperature (O.C.T) Compound (Tissue Tek) and frozen at –80 °C. Frozen samples were then sectioned at a thickness of 30  $\mu$ m and stained with DAPI. All samples were imaged using a Nikon TE300 microscope equipped with a 20 $\times$  objective and a DXM 1200 digital camera was used to capture images at a resolution of 3840  $\times$  3072. Ultraviolet light was used to capture DAPI stained nuclei. Cell depth was measured using Image-J software. Briefly, images were first imported, and calibrated according to the scale bar, and then measurements were taken from the edge of the scaffold to the center of the furthest cell nuclei in line with the measurement tool.

#### 2.5. Uniaxial tensile testing

Tensile tests were conducted on all scaffolds to determine whether the properties were conducive for use as a vascular graft. For testing, six specimens ( $n=6$ ) in a “dog bone” shape were punched from electrospun mats (sample size: 2.75 mm wide at their narrowest point with a length of 7.5 mm) and before testing were hydrated in PBS for 6 h. Uniaxial tensile testing was performed on a MTS Bionix 200 testing system with a 100 N load cell (MTS Systems Corp.) with an extension rate of 10.0 mm/min. Modulus, peak stress, and strain at break were calculated using Test Works version 4.

#### 2.6. Suture retention

Due to the electrospun fibers to form a non-woven fibrous scaffolding on enhanced porosity for use in vascular tissue engineering, this may raise concerns on the ability to retain a suture upon implantation as a bioresorbable vascular prosthetic. Thus, the ability for suture retention was investigated. Suture retention strength was measured on grafts with a rectangular test sample (size: 10 mm in width by 20 mm in length). Before testing, one end of the graft was clamped to one arm of micro material testing machine (MMT-250N, Shimadzu Co., Japan). A loop of a 5-0 polyester suture (Shanghai Pudong Jinhuan Medical Products Co., Ltd, China) was placed 2 mm from the edge of the free end of the sample and clamped to the other arm which moved at a constant speed of 120 mm/min until failure [22]. The suture retention strength was defined as the peak force obtained during the procedure ( $n=6$  for each graft type). All samples were kept hydrated throughout the testing protocols.

#### 2.7. Burst pressure

The burst pressure of a vascular scaffold is one of the most important parameters, the burst pressure strength determine the

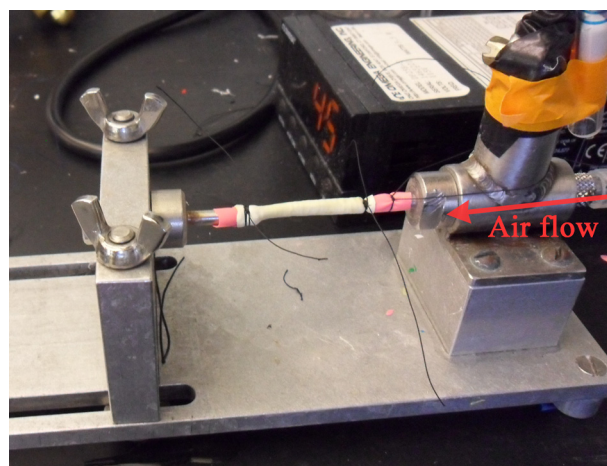


Fig. 2. Image of burst pressure strength device. Air flows from a pressure regulator into grafts, and graft pressure is measured with a pressure transducer.

suitability of scaffold use as a vascular graft for implantation. Burst strength testing of electrospun scaffolds was completed using six different ( $n=6$ ) grafts and a device designed in accordance with section 8.3.3.3 of ANSI/AAMI VP20:1994.31,32 [24]. Tubes, 4 cm in length, were hydrated in PBS for 6 h, fitted over 2.5 mm diameter nipples attached to the device, a thin latex balloon (Party Like Crazy, Target) was inserted, and the balloon/scaffold was secured with 2-0 silk suture to the nipples (Fig. 2). Pressurized air was introduced into the system, increasing the pressure at a rate of 5 mmHg/s until the tubes ruptured. Burst pressure (mmHg) were recorded when the structures ruptured.

#### 2.8. Dynamic compliance

As vascular scaffolds, it is required to be elastic to match the compliance of native blood vessels. Dynamic compliance was determined for tubular grafts taken from six different electrospun grafts ( $n=6$ ) at a length of 4 cm under simulated physiological conditions in accordance with Section 8.10 of ANSI/AAMI VP20:1994.32,33 [24]. Grafts were soaked in PBS for 6 h before testing. The specimens were tested in a bioreactor developed by Tissue Growth Technologies (Minnetonka, MN) filled with PBS. The bioreactor provided a cyclic (1 Hz, representing 60 beats per minute) pressure change to the inside of the graft at a pressure level of 120/80 mmHg systolic/diastolic. Prior to compliance measurements, all grafts were allowed to stress relax for 600 cycles. Internal pressure was measured with a pressure transducer capable of measuring dynamic pressure up to 200  $\pm$  2 mmHg, while the external diameter of the graft was recorded with a laser micrometer system with an accuracy of  $\pm$ 0.001 mm. Compliance was calculated from recording of pressure and inner diameter as:

$$(1)\% \text{ compliance} = \frac{R_{P_2} - R_{P_1}}{R_{P_1}} \cdot \frac{1}{P_2 - P_1} \times 10^4$$

while  $R$  is the internal radius,  $P_1$  is the lower internal pressure, and  $P_2$  is the higher internal pressure.

#### 2.9. Statistics analysis

All the data were obtained at least in triplicate and expressed as means  $\pm$  standard deviation (SD). One-way ANOVA at a significance of  $p < 0.05$  was performed using Origin 8.0 (Origin Lab, USA).

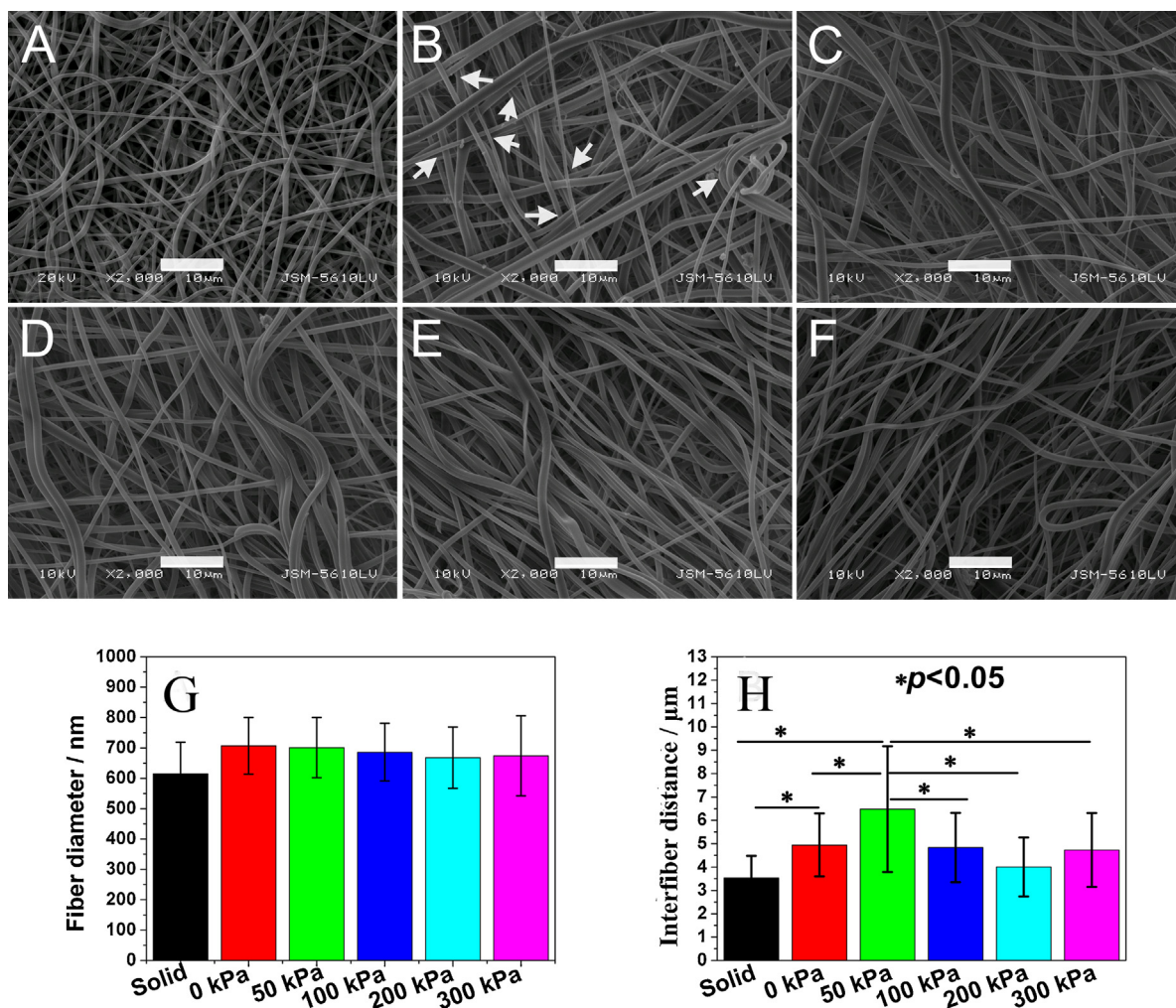


**Fig. 3.** SEM micrographs of scaffold fiber morphology. (A) Fibers deposited on the solid mandrel. ((B)–(F)) Fibers deposited on perforated mandrel with an applied air pressure of 0, 50, 100, 200, 300 kPa, respectively. (G) Fiber diameter results on the specified scaffolds produced. (H) Interfiber distance results for different scaffolds. ((A)–(F)) 2000× magnifications, scale bar = 10 μm. (B) The inserted white arrow area indicates that fibers are crossed or knotted).

### 3. Results

#### 3.1. Scaffold characterization

The morphology of P(LLA-CL)/SF fibers collected separately on the perforated and traditional solid mandrel was observed under SEM and shown in Fig. 3. In Fig. 3A, the fibers deposited on a traditional solid mandrel (scaffold was named “solid” in the full paper) were acquired with the fiber diameter of  $615 \pm 104$  nm (Fig. 3G) and interfiber distance of  $3.5 \pm 1.0$  μm (Fig. 3H). The fibers deposited on perforated mandrel with air flow pressure of 0, 50, 100, 200, 300 kPa (in this full paper, scaffolds were named 0, 50, 100, 200 and 300 kPa, respectively) are shown in Fig. 3(B–F) with fiber diameter of  $707 \pm 93$ ,  $701 \pm 99$ ,  $686 \pm 95$ ,  $668 \pm 101$  and  $674 \pm 132$  nm (Fig. 3G), respectively. The measurement of interfiber distance (inside of the pore region) for those scaffolds produced by air-impedance electrospun (0–300 kPa) is shown in Fig. 3H, with interfiber distance of  $4.9 \pm 1.3$ ,  $6.5 \pm 2.7$ ,  $4.8 \pm 1.5$ ,  $4.0 \pm 1.3$  and  $4.7 \pm 1.8$  μm, respectively. Fig. 3H displayed that the 50 kPa with largest interfiber distance was significantly different ( $p < 0.05$ ) from other scaffolds, and the 0 kPa also has a significantly different ( $p < 0.05$ ) from solid.

With the aim of measuring the mandrel and air pressure impact on the fiber orientation and alignment, we measured scaffolds using the 2D FFT approach with the results presented in Fig. 4. The

FFT of an original data image containing random fibers (Fig. 4A) which deposited on solid mandrel generates an output image containing pixels distributed in a circular shape (Fig. 4C). This distribution means the frequency at which specific pixel intensities occur in the data image is theoretically identical in any direction. In contrast, the FFT of a data image containing aligned fibers (Fig. 4B) which deposited on perforated mandrel (inside of pore region) with air pressure of 300 kPa generates an output image containing pixels distributed in a non-random distribution (Fig. 4D). This distribution occurs because the pixel intensities are preferentially distributed with a specific orientation. The amount of alignment present in the original data images is reflected by the height and overall shape of the peak present in this plot (Fig. 4E and F). For aligned fibers (300 kPa), there are two main peaks at  $38^\circ$  and  $218^\circ$  (Fig. 4F), which show most of the fibers distributed in one direction. In contrast, the random fibers (solid) distributed in any direction, thus more than two peaks are presented in Fig. 4E.

#### 3.2. Cellular infiltration

SMCs were seeded on the scaffolds to study cellular infiltration. As demonstrated by the micrographs in Fig. 5, all of the air-impedance grafts enhanced cellular migration and infiltration. However, cells seeded on the solid grafts were confined to the graft surface and did not infiltrate into the scaffold. The air-impedance

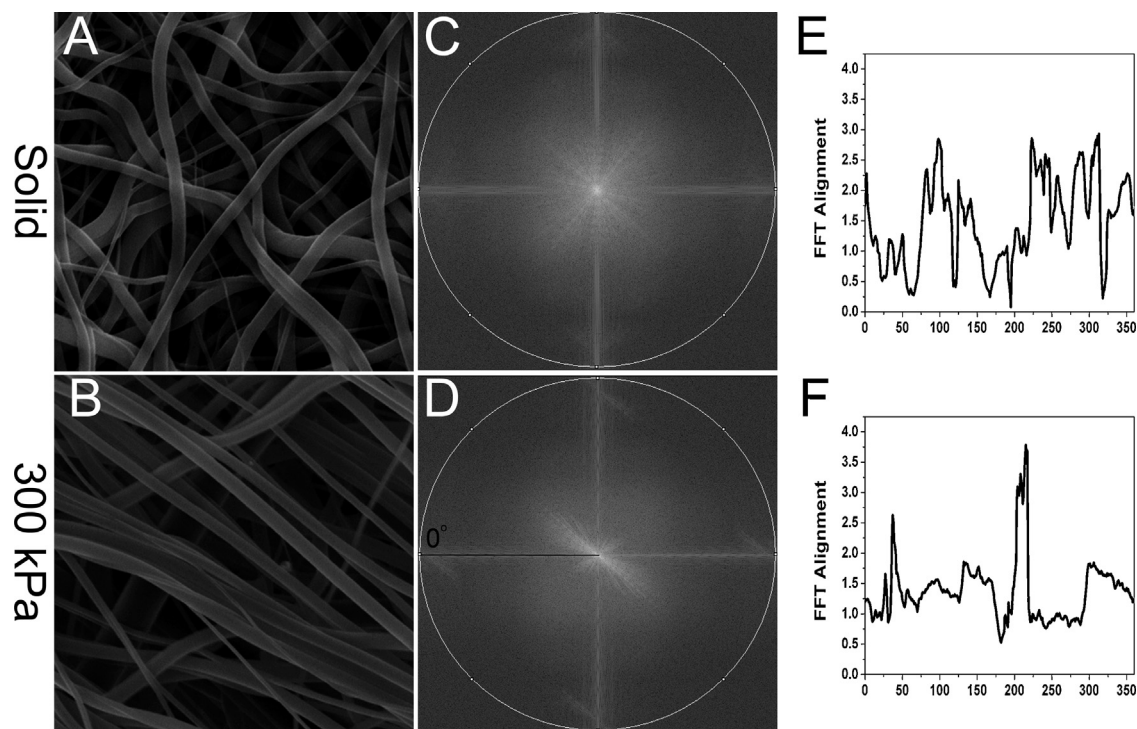


**Fig. 4.** 2D FFT analysis results of scaffold anisotropy. Representative SEM images of solid scaffold (fibers deposited on solid mandrel) (A) and air-impedance scaffold within pore region (300 kPa) (B). FFT output image ((C) and (D)) and 2D FFT alignment plots ((E) and (F)) for the corresponding SEM images. Note the peak position in the 2D FFT alignment plot reports the principle axis of orientation for the fiber field.

scaffolds (from 0 to 300 kPa) all had apparent cellular infiltration (Table 1), with the average depth of  $52 \pm 7$ ,  $137 \pm 8$ ,  $82 \pm 12$ ,  $78 \pm 17$ , and  $96 \pm 26 \mu\text{m}$  at 14 days, respectively.

### 3.3. Tensile testing & suture retention strength

The tensile testing results are shown in Table 2. It revealed that after fabrication by the air-impedance procedure, the peak stress of the electrospun mats with an applied air pressure of 0 and 50 kPa has significantly ( $p < 0.05$ ) increased ( $11.1 \pm 1.0$  and  $12.1 \pm 0.2$  MPa, respectively) relative to the solid mandrel ( $7.6 \pm 0.5$  MPa). When continuing to increase the applied air pressure, the peak stress did not significantly increase. As for the strain at break data, the 0 kPa grafts had a significantly reduced value (143%) compared to others. While the remainder of the strain at break data results showed

that the air-impedance grafts (50–300 kPa) had no significant difference between each other, as well as the solid. Comparing elastic modulus, the 0 and 50 kPa grafts had a significantly higher ( $p < 0.05$ ) modulus value (10.4 and 8.2 MPa, respectively) compared to others. The grafts of 100–300 kPa had no significant difference between each other, as well as the solid.

The ability for suture retention was investigated with the results presented in Table 2. The results showed that the solid mandrel grafts had an average value of  $2.0 \pm 0.5$  N, and air-impedance electrospun grafts from 0 to 300 kPa applied air pressure have average values of  $3.1 \pm 0.6$ ,  $2.8 \pm 0.4$ ,  $2.6 \pm 0.2$ ,  $2.7 \pm 0.2$ , and  $2.5 \pm 0.3$  N, respectively. Overall, the air-impedance grafts have a bit higher suture retention strength than that of the solid.

### 3.4. Burst pressure & dynamic compliance

The burst pressure results are presented in Fig. 6A. Overall, the air-impedance fabrication method with increasing applied air pressure significantly reduced (non-linear) the graft burst pressure strength. The burst pressure of the air-impedance grafts trended lower than solid grafts, with the grafts of 100 kPa and 200 kPa being significant decreased ( $p < 0.05$ ) from other grafts. More specifically, the air-impedance grafts with an applied air pressure from 0 to 300 kPa had burst pressures of  $2732 \pm 21$ ,  $2359 \pm 95$ ,  $1700 \pm 47$ ,  $1780 \pm 108$ ,  $2431 \pm 166$  mmHg, respectively, and the solid grafts possess a burst pressure of  $2774 \pm 93$  mmHg. (Mandrels in this paper with diameter of 6 mm were used, while scaffolds were taken off from mandrel had different degrees of shrinkage, and the inner diameter of grafts were 4–5 mm. Thus, the tubular diameter for all scaffolds was normalized and calculated as 3 mm (saphenous vein has inner diameter about 3 mm) according to Barlow's Formula [24].)

Dynamic compliance testing was conducted with the results presented in Fig. 6B. It showed the compliance of the solid grafts

**Table 1**

Average depth results of cellular penetration. Smooth muscle cells (SMC)-seeded scaffolds with different mandrel conditions after 1, 7 and 14 days of *in vivo* culture.

Mandrel condition	Depth of cellular penetration ( $\mu\text{m}$ )		
	Day 1	Day 7 <sup>a</sup>	Day 14 <sup>a</sup>
Solid	<10	<20	<20
0 kPa	<10	$35 \pm 5$	$52 \pm 7^\dagger$
50 kPa	$41 \pm 6$	$84 \pm 11^*$	$137 \pm 8^\dagger$
100 kPa	$28 \pm 3$	$55 \pm 10$	$82 \pm 12^\dagger$
200 kPa	$32 \pm 6$	$39 \pm 4$	$78 \pm 17^\dagger$
300 kPa	$27 \pm 3$	$63 \pm 10^{**}$	$96 \pm 26^\#$

<sup>a</sup> The statistical significance was compared with air impedance grafts in day 7 and day 14.

<sup>\*</sup> Have a significant difference from others.

<sup>\*\*</sup> Have a significant difference from others except 100 kPa.

<sup>†</sup> Have a significant difference from 0 kPa and 50 kPa. For each group corresponding grafts compared between day 7 and day 14.

<sup>‡</sup> Have significant growth from day 7 to day 14 ( $p < 0.05$ ).

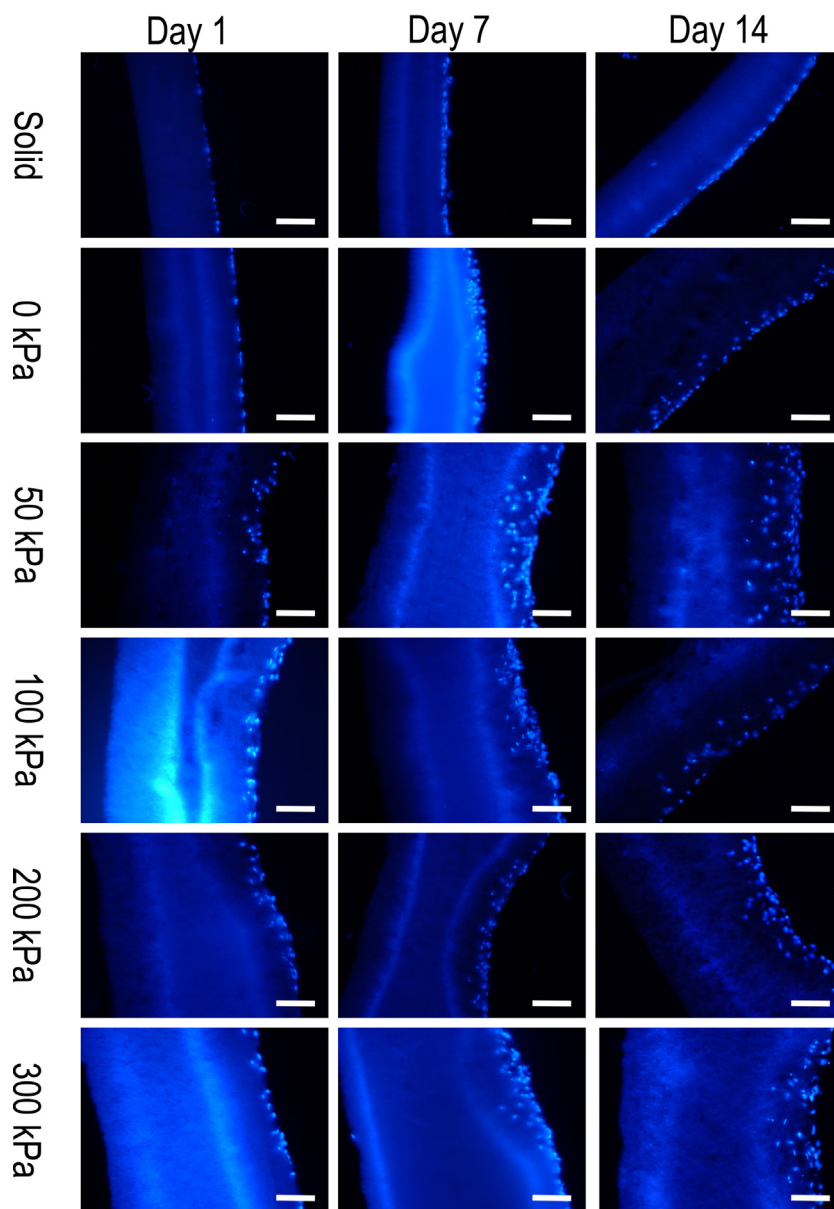


**Fig. 5.** Fluorescence microscopy images of cell infiltration over a period of 1, 7 and 14 days. All images are displayed using a 200 $\times$  magnification (scale bar = 100  $\mu$ m).

( $1.9 \pm 0.4\%$ ) and air-impedance graft of 0 kPa ( $1.9 \pm 0.3\%$ ) were lower than (without significant difference) air-impedance grafts of 50, 100, 200, and 300 kPa. More specifically, the air-impedance grafts produced with an applied air pressure of 50–300 kPa had an average compliance value of  $2.2 \pm 0.1$ ,  $2.4 \pm 0.2$ ,  $2.3 \pm 0.3$ ,  $2.5 \pm 0.2\%$ , respectively, with none of these grafts significantly different from each other. Overall, the results indicate that air-impedance could enhance scaffold dynamic compliance.

#### 4. Discussion

Electrospinning is a versatile process, which can rapidly and easily fabricate tissue engineering scaffolds. Electrospun fibrous scaffolds can simulate the extracellular matrix structure of native tissue in both structure and composition. Unfortunately, the dense packing of the fibrous network impedes cellular infiltration. In order to obtain functional tissue engineered products, it is highly

**Table 2**  
Mechanical properties results of scaffolds with different mandrel conditions.

Mandrel condition	Thickness (mm)	Modulus (MPa)	Peak stress (MPa)	Strain at break (%)	Suture strength (N)
Solid	$0.17 \pm 0.03$	$6.6 \pm 0.8$	$7.6 \pm 0.5$	$169 \pm 14$	$2.0 \pm 0.5$
0 kPa	$0.18 \pm 0.02$	$10.4 \pm 1.0$	$11.1 \pm 1.0$	$143 \pm 12$	$3.1 \pm 0.6$
50 kPa	$0.18 \pm 0.02$	$8.2 \pm 0.6$	$12.1 \pm 0.2$	$204 \pm 15$	$2.8 \pm 0.4$
100 kPa	$0.18 \pm 0.03$	$6.0 \pm 0.9$	$8.1 \pm 0.8$	$189 \pm 11$	$2.6 \pm 0.2$
200 kPa	$0.17 \pm 0.01$	$5.9 \pm 0.9$	$8.7 \pm 0.2$	$207 \pm 23$	$2.7 \pm 0.2$
300 kPa	$0.17 \pm 0.01$	$5.7 \pm 0.4$	$8.1 \pm 0.4$	$202 \pm 7$	$2.5 \pm 0.3$

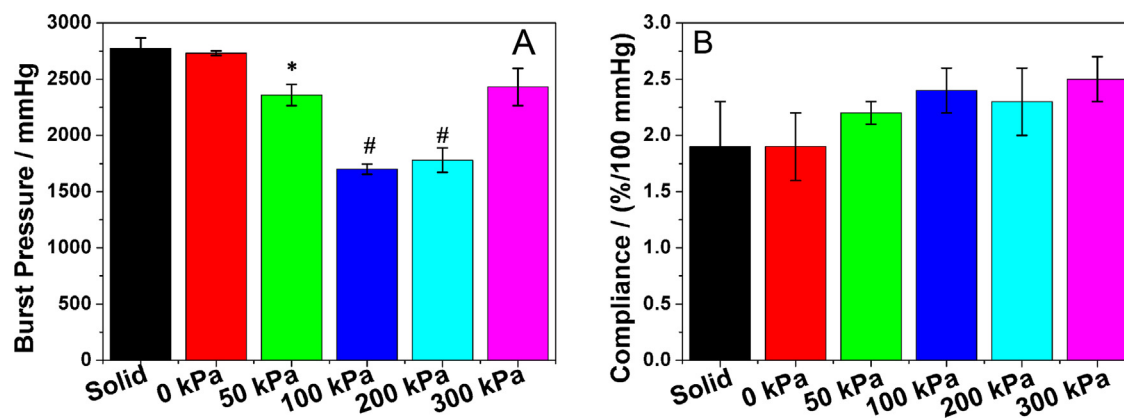


**Fig. 6.** Burst pressure (A) and compliance (B) results of the P(LLA-CL)/SF scaffolds with different processing conditions and mandrels. \* indicates a significant difference from the solid grafts ( $p < 0.05$ ), # indicates a significant difference from solid and air impedance grafts (0, 50, 300 kPa) ( $p < 0.05$ ).

believed that a three-dimensional scaffold will require cells infiltration and migration within the scaffold. Thus, the significant efforts have been made over the past decade at improving the cellular interaction and infiltration of electrospun tissue engineering scaffolds.

In this study, P(LLA-CL)/SF vascular scaffolds were fabricated for potential use in vascular tissue engineering. These vascular grafts, as a bioresorbable prosthetic capable of *in situ* regeneration, were processed through air-impedance electrospinning. In general, it is evident that fibers deposited on the perforated mandrel (Fig. 3B–F) resulted in less compacted fiber deposition. In addition, the uniformity of fiber alignment increased in the pore region with the increasing applied air pressure (Fig. 4). In contrast, the randomly oriented fibers which were deposited on the traditional solid mandrel appeared very compacted. The interfiber distance measurement results (Fig. 3H) revealed that the 50 kPa grafts had significantly larger interfiber distance when compared to other grafts. Perforated mandrel and air pressure appeared to have an effect on interfiber distance as well as fiber alignment. It is hypothesized that, under the effects of the local electrostatic forces within each pore region and pressurized air flow deposition impedance that the fibers were deposited onto mandrel are less compacted regionally. Meanwhile, as the air pressure increased, the fiber alignment increased, while the interfiber distance trended to reducing.

As noted, the degree of cellular infiltration is a critical property of a scaffold to create a functional, 3-D tissue. Previous study indicated that P(LLA-CL)/SF electrospun nanofibrous scaffold possessed good biocompatibility, it promoted cells growth significantly comparison with P(LLA-CL), however, the cellular infiltration were hindered due to the small interfiber distance of scaffolds [30]. The results of this study demonstrate an improvement in cellular infiltration with air-impedance processing of the grafts (Fig. 5 and Table 1), particularly in the air-impedance graft of 50 kPa. This is in dramatic contrast to the solid where the cells attached on the surface of the scaffold and remained as a confluent layer of cells on the scaffold surface. According to the literature, the architectural features of scaffold could affect the cells behavior [31–34]. It is hypothesized that cell infiltration can be influenced by two factors. If the scaffold possesses large interfiber distance, cells could infiltrate deep into the scaffold independent of fiber alignment. Among the scaffolds mentioned by this study, the 50 kPa graft had the largest interfiber distance and promoted the deepest penetration of cells into the scaffold. On the other hand, it was noticed that an increase in air pressure resulted in increasing fiber alignment and reduced interfiber distance (200 and 300 kPa). The depth of cellular infiltration for air-impedance grafts (200, 300 kPa) are deeper than solid and

0 kPa grafts. Although the interfiber distance of these grafts has no significant difference, the fiber alignment for 200, 300 kPa scaffolds are higher. It is suggested that cells appeared as spindle like shape and elongated along with the aligned fiber so that cells could penetrated along the gap of the parallel fibers. While as for the solid scaffold, fibers are randomly oriented, have a smaller interfiber distance, and are very compacted. As a result, the cells spread fluent on the fiber and were confined to the surface of scaffold.

As the electrospun scaffolds were modified by the induced air flow, there was concern that the affects could have lead to the deterioration of the overall structure's mechanical properties and structural integrity. Thus, we conducted comprehensive evaluations of the scaffold's mechanical properties in terms of tensile testing, suture retention, burst pressure, and dynamic compliance. It is evident that the mandrel and air pressure affected the grafts' mechanical properties.

Fibers deposited on the solid mandrel were randomly oriented, while the fibers deposited on the perforated mandrel are not as random as on solid mandrel due to the different local electrostatic forces on the perforated mandrel (without air pressure), and the fibers are crossed and knotted partially (see Fig. 3B). As the air pressure increased, the fibers became more aligned. Thus, when the scaffolds are stretched, part of strength will concentrated on the knotting (0 kPa), so it is difficult to stretch but will break abruptly. As a result, we noticed that the stress of 0 kPa was very higher than solid grafts while the strain was lower. When air pressure is increased, the fiber knotting will be reduced (50 kPa). Therefore, when the scaffold is stretched, the stress is still large but it will not break as abruptly as 0 kPa. This result in a higher strain for 50 kPa than 0 kPa, however, the modulus will reduce. As air pressure continues to increase, the fibers orientation will be defined and become increasingly aligned (from 100 to 300 kPa), thus most of the fibers will be stretched along the same direction when subjected to tensile load. Therefore, those scaffolds should possess higher strain, moderate stress (lower than 0 and 50 kPa but higher than solid one) and low modulus. The suture retention strength of all scaffolds has the same tendency with their stress. For vascular prosthetic applications such as a small diameter artery, the tensile strength required to withstand the intraluminal blood pressure is 4.4 MPa, thus all of the scaffold fabricated in this study have satisfied this requirement [22,35,36], and the ultimate strain of these scaffolds was comparable to the human artery (45–99%) [37]. Although the modulus is still stiffer than the native artery ( $2.68 \pm 1.81$  MPa) [38], previous study showed the modulus will be decreased with bulk degradation of the electrospun porous scaffolds, and even faster when implanted *in vivo* [39]. For cardiovascular tissue engineering, it is very important to retain strength until the ECM remodeled for withstanding

the physiological load. Additionally, the air-impedance grafts possessed suture retention strengths greater than 2 N, which is greater than the values for native blood vessels (suture retention strength value of 1.7 N) [22], therefore, the suture retention strength of the scaffold be sufficient for use in a surgical procedure.

With the air flow out of the pore of mandrel, the fibers deposited onto the perforated mandrel loosely while compactly on solid mandrel, thus for burst pressure resistance, the tubular scaffolds collected on perforated mandrel were weaker than on that of solid mandrel. While for the compliance, the effect will be just opposite, the air-impedance tubular scaffolds had a higher compliance than that of solids. This is attributed to the higher air pressure causing an increase in fiber alignment. The saphenous vein is considered the gold standard for small diameter vascular grafting procedures with this vessel possessing a burst pressure strength of approximately 1600 mmHg [3,6,40]. Thus the air-impedance electrospun grafts have potential for surgical procedures to replace the saphenous vein and non-absorbable vascular prosthetics. After inducing the air pressure, the results showed the compliance of the air-impedance grafts improved and were higher compared to the saphenous vein (0.7–1.5%/100 mmHg) [41], meanwhile the values of compliance were approximately 2%/100 mmHg which is very close to that of native tissue (2.6%/100 mmHg) [40–42].

## 5. Conclusion

This study demonstrated that the mandrel architecture and air pressure affect the fiber deposition, fiber alignment, and the interfiber distance of scaffold. Fibers deposited onto perforated mandrels possess larger interfiber distances than on solid mandrels. Additionally, the high air pressure caused aligned fiber deposition which resulted in enhanced cellular infiltration for air-impedance electrospun scaffolds. Meanwhile the air-impedance scaffold still possessed adequate mechanical properties such as tensile strength, suture retention strength, burst pressure and compliance which are very close to that of native tissue. Thus, this type of scaffold may be useful in applications such as biodegradable vascular substitutes.

## Acknowledgments

This work was supported by National Natural Science Foundation of China (31070871, 31271035), Science and Technology Commission of Shanghai Municipality (11nm0506200), the National Plan for Science and Technology (10-NAN1013-02), Research grant no. RGP-VPP-089, the Doctoral Innovation Fund of Donghua University (BC201127) and visiting professor program from King Saud University.

## References

[1] V.L. Roger, A.S. Go, D.M. Lloyd-Jones, E.J. Benjamin, J.D. Berry, W.B. Borden, D.M. Bravata, S. Dai, E.S. Ford, C.S. Fox, H.J. Fullerton, C. Gillespie, S.M. Hailpern, J.A. Heit, V.J. Howard, B.M. Kissela, S.J. Kittner, D.T. Lackland, J.H. Lichtman, L.D. Lisabeth, D.M. Makuc, G.M. Marcus, A. Marelli, D.B. Matchar, C.S. Moy, D. Mozaffarian, M.E. Mussolino, G. Nichol, N.P. Paynter, E.Z. Soliman, P.D. Sorlie, N. Sotoodehnia, T.N. Turan, S.S. Virani, N.D. Wong, D. Woo, M.B. Turner, *Circulation* 125 (2012) e2.

[2] B.C. Isenberg, C. Williams, R.T. Tranquillo, *Circ. Res.* 98 (2006) 25.  
 [3] V.A. Kumar, L.P. Brewster, J.M. Caves, E.L. Chaikof, *Cardiovasc. Eng. Technol.* 2 (2011) 137.  
 [4] D. Liao, X. Wang, P.H. Lin, Q. Yao, C.J. Chen, *J. Cell. Mol. Med.* 13 (2009) 2736.  
 [5] B. Tschoeke, M. Sriharwoko, V. Ella, S. Koch, A. Glitz, T. Schmitz-Rode, T. Gries, M. Kellomaki, S. Jockenhoevel, *Tissue Eng.* 13 (2007) 1770.  
 [6] N. L'Heureux, S. Paquet, R. Labbe, L. Germain, F.A. Auger, *FASEB J.* 12 (1998) 47.  
 [7] J.D. Schiffman, C.L. Schauer, *Polym. Rev.* 48 (2008) 317.  
 [8] A. Yin, K. Zhang, M.J. McClure, C. Huang, J. Wu, J. Fang, X. Mo, G.L. Bowlin, S.S. Al-Deyab, M. El-Newehy, *J. Biomed. Mater. Res. A* 101 (2013) 1292.  
 [9] E.D. Boland, J.A. Matthews, K.J. Pawlowski, D.G. Simpson, G.E. Wnek, G.L. Bowlin, *Front. Biosci.* 9 (2004) 1422.  
 [10] K. Zhang, Y. Qian, H. Wang, L. Fan, C. Huang, A. Yin, X. Mo, *J. Biomed. Mater. Res. A* 95 (2010) 870.  
 [11] J. Ayutse, M. Gandhi, S. Sukigara, H.H. Ye, C.M. Hsu, Y. Gogotsi, F. Ko, *Biomacromolecules* 7 (2006) 208.  
 [12] K.H. Zhang, A.L. Yin, C. Huang, C.Y. Wang, X.M. Mo, S.S. Al-Deyab, M. El-Newehy, *Polym. Degrad. Stab.* 96 (2011) 2266.  
 [13] N. Bhattarai, D. Edmondson, O. Veiseh, F.A. Matsen, M. Zhang, *Biomaterials* 26 (2005) 6176.  
 [14] J. Zeng, X. Xu, X. Chen, Q. Liang, X. Bian, L. Yang, X. Jing, *J. Controlled Release* 92 (2003) 227.  
 [15] T. Yokota, H. Ichikawa, G. Matsumiya, T. Kuratani, T. Sakaguchi, S. Iwai, Y. Shirakawa, K. Torikai, A. Saito, E. Uchimura, N. Kawaguchi, N. Matsuura, Y. Sawa, *J. Thorac. Cardiovasc. Surg.* 136 (2008) 900.  
 [16] R.A. Pullens, M. Stekelenburg, F.P. Baaijens, M.J. Post, *J. Tissue Eng. Regen. Med.* 3 (2009) 11.  
 [17] S.H. Lim, S.W. Cho, J.C. Park, O. Jeon, J.M. Lim, S.S. Kim, B.S. Kim, *J. Biomed. Mater. Res. B Appl. Biomater.* 85 (2008) 537.  
 [18] B.W. Tillman, S.K. Yazdani, S.J. Lee, R.L. Geary, A. Atala, J.J. Yoo, *Biomaterials* 30 (2009) 583.  
 [19] E.D. Boland, B.D. Coleman, C.P. Barnes, D.G. Simpson, G.E. Wnek, G.L. Bowlin, *Acta Biomater.* 1 (2005) 115.  
 [20] M.J. Smith, M.J. McClure, S.A. Sell, C.P. Barnes, B.H. Walpoth, D.G. Simpson, G.L. Bowlin, *Acta Biomater.* 4 (2008) 58.  
 [21] X.M. Mo, C.Y. Xu, M. Kotaki, S. Ramakrishna, *Biomaterials* 25 (2004) 1883.  
 [22] H. Bergmeister, C. Schreiber, C. Grasl, I. Walter, R. Plasenzotti, M. Stoiber, D. Bernhard, H. Schima, *Acta Biomater.* 9 (2013) 6032.  
 [23] P. Zilla, D. Bezuidenhout, P. Human, *Biomaterials* 28 (2007) 5009.  
 [24] M.J. McClure, P.S. Wolfe, D.G. Simpson, S.A. Sell, G.L. Bowlin, *Biomaterials* 33 (2012) 771.  
 [25] Y.M. Ju, J.S. Choi, A. Atala, J.J. Yoo, S.J. Lee, *Biomaterials* 31 (2010) 4313.  
 [26] J. Wu, S. Liu, L. He, H. Wang, C. He, C. Fan, X. Mo, *Mater. Lett.* 89 (2012) 146.  
 [27] B.M. Baker, A.O. Gee, R.B. Metter, A.S. Nathan, R.A. Marklein, J.A. Burdick, R.L. Mauck, *Biomaterials* 29 (2008) 2348.  
 [28] H.J. Jin, J.S. Chen, V. Karageorgiou, G.H. Altman, D.L. Kaplan, *Biomaterials* 25 (2004) 1039.  
 [29] C. Ayres, G.L. Bowlin, S.C. Henderson, L. Taylor, J. Shultz, J. Alexander, T.A. Telemeo, D.G. Simpson, *Biomaterials* 27 (2006) 5524.  
 [30] K. Zhang, H. Wang, C. Huang, Y. Su, X. Mo, Y. Ikada, *J. Biomed. Mater. Res. A* 93 (2010) 984.  
 [31] C. Xu, *Biomaterials* 25 (2004) 877.  
 [32] J.S. Choi, S.J. Lee, G.J. Christ, A. Atala, J.J. Yoo, *Biomaterials* 29 (2008) 2899.  
 [33] A.J. Meinel, K.E. Kubow, E. Klotzsch, M. Garcia-Fuentes, M.L. Smith, V. Vogel, H.P. Merkle, L. Meinel, *Biomaterials* 30 (2009) 3058.  
 [34] C. Vaquette, C. Kahn, C. Frochet, C. Nouvel, J.L. Six, N. De Isla, L.H. Luo, J. Cooper-White, R. Rahouadj, X. Wang, *J. Biomed. Mater. Res., A* 94 (2010) 1270.  
 [35] J.P. Theron, J.H. Knoetze, R.D. Sanderson, R. Hunter, K. Mequanint, T. Franz, P. Zilla, D. Bezuidenhout, *Acta Biomater.* 6 (2010) 2434.  
 [36] A. Nieponice, L. Soletti, J.J. Guan, B.M. Deasy, J. Huard, W.R. Wagner, D.A. Vorp, *Biomaterials* 29 (2008) 825.  
 [37] C. Xu, R. Inai, M. Kotaki, S. Ramakrishna, *Tissue Eng.* 10 (2004) 1160.  
 [38] S. Laurent, X. Girerd, J.J. Mourad, P. Lacolley, L. Beck, P. Boutouyrie, J.P. Mignot, M. Safar, *Arterioscler. Thromb. Vasc. Biol.* 14 (1994) 1223.  
 [39] B.L. Dargaville, C. Vaquette, F. Rasoul, J.J. Cooper-White, J.H. Campbell, A.K. Whittaker, *Acta Biomater.* 9 (2013) 6885.  
 [40] S.G. Wise, M.J. Byrom, A. Waterhouse, P.G. Bannon, M.K.C. Ng, A.S. Weiss, *Acta Biomater.* 7 (2011) 295.  
 [41] N. L'Heureux, N. Dusserre, G. Konig, B. Victor, P. Keire, T.N. Wight, N.A. Chronos, A.E. Kyles, C.R. Gregory, G. Hoyt, R.C. Robbins, T.N. McAllister, *Nat. Med.* 12 (2006) 361.  
 [42] R. Roeder, J. Wolfe, N. Lianakis, T. Hinson, L.A. Geddes, J. Obermiller, *J. Biomed. Mater. Res.* 47 (1999) 65.